Current Applied Physics 20 (2020) 470–476

Contents lists available at ScienceDirect

Current Applied Physics

journal homepage: www.elsevier.com/locate/cap

Surface modification of CdSe nanocrystals: Application to polymer solar cell

M. Nabil[a], Shaimaa A. Mohamed[b,c,d,*], K. Easawi[a], Salah S.A. Obayya[c], S. Negm[a], H. Talaat[e], M.K. El-Mansy[f]

[a] Department of Mathematical and Physical Engineering, Faculty of Engineering (Shoubra), Banha University, Cairo, Egypt
[b] Center for Nanotechnology, Zewail City of Science and Technology, October Gardens, 6th of October, Giza, 12578, Egypt
[c] Center for Photonics and Smart Materials, Zewail City of Science and Technology, October Gardens, 6th of October, Giza, 12578, Egypt
[d] Nanotechnology and Nanoelectronics Engineering Program, Zewail City of Science and Technology, October Gardens, 6th of October, Giza, 12578, Egypt
[e] Physics Department, Faculty of Science, Ain Shams University, Abbassia, Cairo, Egypt
[f] Department of Physics, Banha University, Stadium Street, 13518, Banha, Egypt

ARTICLE INFO

Keywords:
Photovoltaic
CdSe nanocrystal
Surface passivation
Iodide ligand

ABSTRACT

The optimum choice of the ligand that stabilizes the colloidal quantum dots and passivate the surface is crucial for tuning the energy level and remain elusive. The atomic ligand passivation with iodide remains superior over other surface treatments. Herein, we applied the iodide ligand to passivate the CdSe nanocrystals with an excitonic absorption at 2.1 eV by a liquid-liquid extraction process. We took the view of the change in the optical and structural properties upon ligand exchange. Finally, we tested the performance of the iodide treated dots by employing it in an inverted structure polymer solar cell based on P3HT: PCBM.

1. Introduction

The needs for alternative clean energy sources ignite the race toward the synthesis and design of efficient sunlight harvesting material. The fast-developing classes for the upcoming technological revolution are those materials that can easily casted into a film from a solution [1–8]. The advantages are being low-cost alternatives for sophisticated high vacuum techniques, and easy scalability into a large area utilizing different coating routes include doctor blading, roll to roll, and inkjet printing. Among these, organic conductive polymer feature a high absorption coefficient of thousand times thinner films compared to the inorganic counterpart. The drawback is their limited efficiency due to the minimal charge generation as well as extraction when assembled in the form of organic photovoltaic device OPV [9]. Many approaches have been adopted to improve the device performance, and interface of the constituent layers include the use of low bandgap polymer, shape the morphology of the active layer through thermal annealing, use dopants to improve the absorptivity and the optimum choice of the electron or hole transport layers at the electrode interface [10–22]. The additive should satisfy two criteria. First, the energy levels should have an appropriate offset concerning the donor and the acceptor. Second, it can be used as an electron acceptor or donor or assist in the charge carrier transport. Subsequently, the highest occupied molecular orbital (HOMO) and the lowest unoccupied molecular orbital (LUMO) of the additive are required to be intermediate to those of the donor and the acceptor, creating a cascade energy band structure [23–26]. Here, especially, QDs has grasped the attention as an additive by their bandgap tunability through the quantum size effect [27–37]. The commonly used QDs are cadmium selenide, which usually prepared by the hot injection methods [38–44]. Upon synthesis, long-chain insulating organic ligands such as tri-n-octylphosphine oxide (TOPO), oleic acid (OA), and hexadecylamine (HDA) usually act as a capping agent for colloidal quantum dots. Although these ligands are essential to achieving the optimum confinements, it represents a barrier against charge carrier transport when employed in the device fabrication. It then creates a trade of case between improving the carrier transport and maintaining the quantum confinements. Recent trends in quantum dot research apply short ligands to replace the long insulating organic capping agent. Among these, atomic ligand passivation with iodide is reported as a superior ligand to passivate the quantum dot surface owing to the high charge carrier mobility and record-holding device efficiency [45–52]. In the present work, we employed iodide as a surface passivation ligand to replace the original starting capping agents, and we traced the change in the material properties upon the ligand exchange process. Finally, we implemented the iodide treated dots in the fabrication of an inverted structure polymer solar cells based on regioregular Poly (3-hexylthiophene-2, 5-diyl) P3HT and Phenyl-C61-butyric acid methyl ester (PCBM) in a ratio of 1:1:1 (P3HT: CdSe:

* Corresponding author. Center for Nanotechnology, Zewail City of Science and Technology, October Gardens, Giza, 12578, Egypt.
E-mail address: smohamed@zewailcity.edu.eg (S.A. Mohamed).

https://doi.org/10.1016/j.cap.2020.01.001
Received 5 November 2019; Received in revised form 22 December 2019; Accepted 1 January 2020
Available online 10 January 2020

PCBM).

2. Materials and methods

2.1. Materials

Cadmium oxide (CdO 99.99%), trioctylphosphine oxide (TOPO 99%) Selenium (99.99%), and trioctyiphosphine (TOP 97%), Hexadecylamine (HDA 98%), Oleic acid (≥99%) and tetra-butylammonium iodide TBAI (≥98%) are received from Sigma Aldrich. Phenyl-C_{61}-butyric acid methyl ester, PCBM ($C_{72}H_{14}O_2$, MW = 910.88, Purity > 99.5%) and regioregular poly (3-hexylthiophene-2, 5-diyl) P3HT (with MW = 50–70 K, purity > 99.5%) are purchased from Solarmer Energy, Inc. An aqueous solution of poly (3, 4-ethylene dioxythiophene) doped with poly (styrenesulfonic acid) (PEDOT: PSS, Baytron/Clevios PH 500) is purchased from Heraeus and filtered (0.45 m Teflon filter) before use. We purchased the Organic solvents from Alfa Aesar. All chemicals are used directly without any further purification.

CdSe Nanocrystal synthesis and ligand exchange: ~5 nm, monodisperse, and highly fluorescent We fabricated the CdSe nanocrystal-based on the modification of those previously reported techniques [53]. For Cd precursor preparation, we used 0.3 g (2.34 mmol) of CdO in 2 g (0.701 mol) oleic acid at 170 °C. A mixture of 2 g (4.77 mmol) of TOPO and 2 g (8 mmol) of HDA is added to the solution and held at 180 °C for nearly 5 min. Meanwhile, Selenium precursor by dissolving a 0.3 g (3.79 mmol) of selenium in 4 mL (8.8 mmol) of TOP. The Cadmium solution is loaded to a tri-neck flask and heated to 130 °C, followed by the injection of the selenium solution dropwise to the reaction mixture and heating to 220 °C for 15 min, during this time CdSe in-situ indicated by the change in color in the reaction mixture. The heating mantle is removed to allow cooling of the three-neck flask to 100 °C then reinstalled to keep the bottle flask at 100 °C for approximately 5 min. The reaction is then rapidly quenched by cooling the solution in a water bath. CdSe NCs are washed via dispersion in hexane and ethanol, followed by centrifugation. We repeated the washing steps three times, and upon completion, all solid residues are re-dispersed in hexane. For ligand Substitution: A 0.1 M solution of tetra butyl ammonium iodide (TBAI) in DMF is prepared with the help of sonication and temperature to speed the dissolution. CdSe QDs in hexane of typically ~20 mg/ml is then added and transferred from hexane to DMF by continues shaking for a few minutes. After that, we removed the excess hexane from solution, and we used isopropyl alcohol to deposit the QDs. The deposited CdSe QDs are then collected and dried under the flow of nitrogen and re-dispersed in dichlorobenzene for device fabrication.

2.2. Characterization

The optical absorption spectra in the wavelength range between 250 and 800 nm are recorded in a quartz cuvette for the colloidal solution or coated on a glass microscope slide for films with the aid of the UV–Vis spectrophotometer (Jasco, Model 670). The emission spectra are carried out using RF-5301PC Spectrofluorophotometer, Shimadzu, operated with a 150W Xenon lamp and with an excitation wavelength of 480 nm. Fourier transforms FTIR spectra are recorded on pressed pellets made of dried CdSe nanocrystals (3 mg) before and after ligand substitution with TBAI at a different time interval of 4, 6, 8 and 24 h using a using 6300 Fourier transform infrared spectrometer in the wavenumber range (400-4000 cm^{-1}). The particle size and shape are determined using a high-resolution transmission electron microscopy (HRTEM, JEOL JEM- 2100 LaB6 operated at 200 KV with high-resolution Gatan CCD bottom camera, Orius SC200 and using the specimen tilt holder EM-31630). For TEM measurements, we spun a thin film of CdSe nanocrystal over a 3 mm mesh size grid made from Cu to support the particles during imaging.

2.2. Solar Cell Fabrication

For the photovoltaic cells, patterned 2.5 cm^2 glass-indium tin oxide (Fluorine doped tin oxide coated glass slides with a sheet resistance of ~7 Ω/square). For glass cleaning, we used a detergent (Hellmanex, Hellma Inc.) at 80 °C, in the ultrasonic bath followed by deionized water for 15 min each. After washing, samples are dried and treated with UV-ozone in a plasma chamber for 15 min. The titanium dioxide layer was prepared from Titanium (IV) isobutoxide precursor in IPA (0.1M) under a nitrogen atmosphere. The Solution is spun on the FTO glass substrate at 10 rps for 2 Sec, followed by 50 rps for 10 Sec. The deposited layer is annealed at 150 °C for 30 min, then left under ambient conditions overnight to allow the growing of the TiO_x layer [54]. Before use, substrates are treated with oxygen plasma at 50 °C then calcination at 500 °C for 1 h. For the active layer, solution of P3HT: PCBM (1:2) in dichlorobenzene with a final concentration of 15 mg L^{-1} is prepared and leftover magnetic stirrer at 60 ^{O}C overnight and filtered before use. A solution of the iodide treated CdSe quantum dots in dichlorobenzene is prepared and mixed with the P3HT: PCBM solution in a ratio of (1:1). Another solution of P3HT: PCBM is prepared and applied for a reference device. The solution is crusted on the top of the Tio_x layer at 1500 rpm for 15s and aged at 60 °C for 10 min under a flow of nitrogen. The thermal deposition of MoO_3/Ag completes the final device assembly as a top metal contact. Solar cells based on this structure are prepared in batches of (12 devices) for both reference devices, and those contain CdSe QDs. The photovoltaic cells are characterized in dark and under1 Sun solar simulator irradiation (100 mW/cm^2, Newport). A keithley 2400 source meter is used to record the current density-voltage J-V characteristics. The external quantum efficiency (EQE) is marked with a wavelength step of 5 nm from 350 to 800 nm using monochromatic light, and Si detector used for system calibration. The short circuit current Jsc values are derived by integrating spectral EQEs and corrected in all J-V plots and tables accordingly.

3. Results and discussion

In the present study, we took the view into ~ 5 nm CdSe colloidal quantum dots that are originally capped with TOPO/HDA and we trace the changes in the optical and structural properties upon ligand exchange with the iodide ligand with a final goal to use it as an additive in polymer solar cells based on P3HT: PCBM (See Fig. 1). The absorption and emission properties are presented in Fig. 2a and showed a preserved excitonic absorption and emission peaks, which indicate that the QDs are remaining in the confined regime with a slight red shift in the emission from (2.05–2.02 eV) when the dots come closer (See the supporting information S1). Fig. 2b shows the TEM image (100 nm Scale bar) and the size distribution for the quantum dots (tiny dark dots with tail ligand) before and after iodide substitution. The as-synthesized Qds appear highly monodisperse with a size distribution centered at ~5 nm and relatively large spacing between particles results from the original bulky ligand used for the quantum dots growth [1.1 nm, 0.98 nm and 0.9 nm corresponding to TOPO, HDA and OA respectively [55]. Iodide passivation on the other hand, offered scale size down to 0.1 nm denoted as atomic ligand passivation in literature and resulted in high densely packing nanocrystals with small interatomic spacing [45–52]. Similar observations have been studied in different systems including short mono- and a bidentate organic ligand. For example, ethanedithiol EDT ligand treatment of PbS nanocrystals results in the center-to-center spacing of 1.6 nm in the EDT treated films corresponds to the untreated one [56]. The reduction of the particle size could be due to the loss of a certain amount of Cd and Se (one or two atomic layers on the surface) upon ligand exchange. Talapin et al. reported a similar observation for pyridine treated CdSe QDs of particle size (3–4 nm) compared to TOPO-CdSe QDs (5–6 nm) [57].

We are then employed the Tauc's equation (Eq. 1) to track the

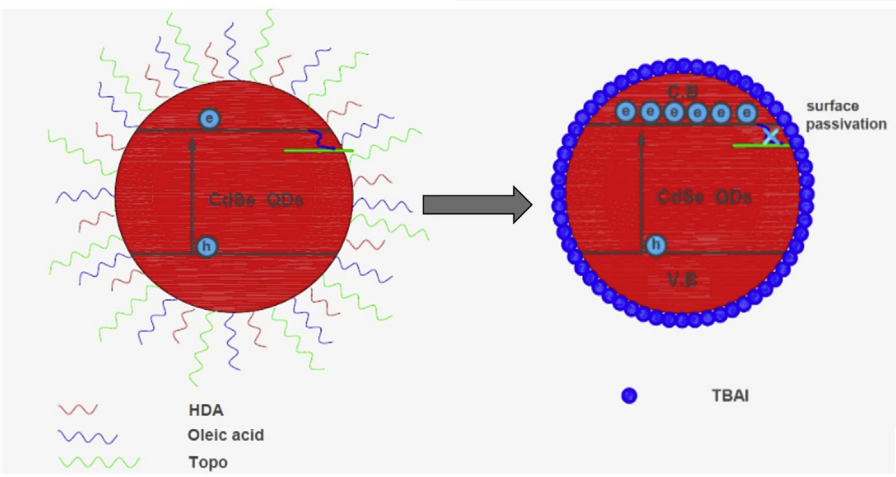

Fig. 1. Cartoon drawing for the as-synthesized CdSe QDs and the Iodide treated dots.

changes in the energy bandgap of the CdSe nanocrystals upon iodide ligand exchange.

$$\alpha h\upsilon = A(h\upsilon - E_g)^n \tag{1}$$

Where (*A)* is constant (α) is the optical absorption coefficient, $(h\nu)$ is the energy of the incident photons, (*h)* is Planck's constant and *n* value depends on the optical transition type (direct or indirect electronic transition). *n* takes the values (1/2,3/2) for direct allowed, direct forbidden, and value (2,3) for indirect allowed and indirect forbidden transitions, respectively. In the case of CdSe QDs, the transition is an indirect allowed semiconductor, and *n* value is chosen to be *2*. The Tauc's plot of $(\alpha h\nu)^2$ versus $(h\nu)$ Shows an intermediate linear region (See the supporting information S2) and is used to extract the energy bandgap from the extrapolation of the linear part with the x-axis, which is found to be 2.05 eV and 2.07 eV for TOPO/HDA and Iodide respectively. The calculated band gaps are then used to estimate the particle sizes according to two different models, the Effective Mass Approximation model (EMA) and the Polynomial Fitting Functions (*PFF*). The particle size is calculated based on the effective mass approximation model according to the following equation Eq. 2 [58];

$$E_{gn} = E_{gb} + \frac{h^2}{8R^2}\left[\frac{1}{m_e} + \frac{1}{m_h}\right] - \frac{1.8e^2}{4\pi\varepsilon\varepsilon_0 R} \tag{2}$$

Where E_{gn} (NC) is the lowest energy electronic transition for nanocrystals, (E_{gb}) is the bandgap of bulk CdSe (1.74 eV), (R) is the average radius of nanoparticles, (m_e) is the effective mass of electron (0.13 m_o), (m_h) is the effective mass of hole (0.45 m_o) and ε is the dielectric constant [59]. While the Polynomial Fitting Functions (*PFF*) applying the below equation Eq. 3 [53]:

$$D = (1.6122 \times 10^{-9})\lambda^4 - (2.657 \times 10^{-6})\lambda^3 + (1.6242 \times 10^{-3})\lambda^2 - (0.4277)\lambda + (41.57) \tag{3}$$

Where *D* (nm) is the size of a given CdSe QDs sample, and λ_{max} (nm) is the wavelength of the optical excitonic peak of the corresponding sample. The extracted values of the particle size in all cases are collected in Table 1 for comparison.

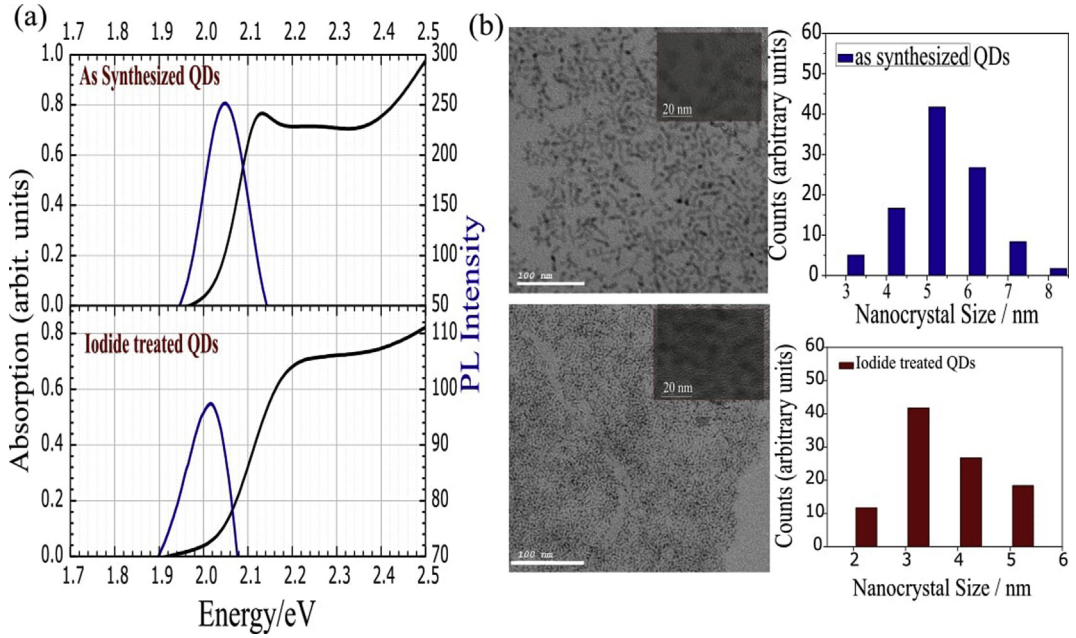

Fig. 2. (a) Plot of the absorption and emission spectra in the energy range of the As-synthesized and iodide treated CdSe nanocrystals exhibit their primary absorption and emission feature according to the quantum size effect. (b) The TEM image (100 nm scale bar, the figure inside is 20 nm scale bar) shows highly monodisperse particles and the corresponding particle distributions. It indicates a reduction in the interatomic spacing and average particle size upon iodide ligand exchange.

Table 1
The calculated particle size of the CdSe QDs before and after ligand treatment as estimated by EMA and PFF methods and as observed by HRTEM.

	1st method (*EMA*) (nm)	2nd method (*PFF*)(nm)	HRTEM (nm)
CdSe QDs/OA,TOPO,HDA	4.02	4.49	4.72
CdSe/Iodide ligand	3.73	4.23	4.25

Since surface passivation determine the quality and performance of the colloidal nanocrystal and crucial for the improvement of the charge carrier mobility, we offer the elaboration of the details changes in the vibrational mode during substitution of the HDA/TOPO ligand with the iodide by looking into account the Fourier transform infrared spectroscopy (FTIR) at different time interval of 4 h, 6 h, and 24 h. The full FTIR spectrum is presented in Fig. 3a. It shows depletion in the peak intensities at 2924, 2857 cm^{-1} that are characterizing the C–H stretching vibration while the band at 1260 cm^{-1} is due to the bending mode of the C–H group. The vibration modes located at 1600 cm^{-1} and 1700 cm^{-1} are finger prints for the C═C and C═O groups. The decrease in the intensities of these two bands upon increasing ligand treatment time and indicate the successive removal of the oleic acid present in the system. The sharp peak at 3300 cm^{-1} arose from the N–H group from the hexadecylamine (HAD) ligand. The washing at the beginning with alcohol results in a broad band at 3000-3700 cm^{-1} of the O–H group. This band is then almost disappeared after long-time treatment [60,61]. Although of the continuous decrease in the peak intensities that are characteristic of the TOPO/HDA/OA with the increase in the iodide treatment time, the final plot still exhibits a week IR vibrational modes related to remaining traces of these primary surfactants. Nevertheless, we see clearly that CdSe quantum dots became capped with the new short iodide ligand Fig. 3b Shows the X-Ray diffraction pattern for the as-synthesized quantum dots and the iodide capped CdSe quantum dots. The width of the diffraction peak appears broader as usually obtained for QDs. The XRD patterns indicate that the QDs exhibit a wurtzite phase. Both CdSe QDs samples showed diffraction peak at 2Θ = 25.19°, 41.94°, 49.83°, the observed peaks are corresponding to (111), (220), and (311) plans of the cubic structure of CdSe QDs. These peaks are well-matched with cubic structure (card No. 01-088-2346), which is in the confirmation of the cubic structure of CdSe crystals. We further observe some additional peaks in the XRD pattern due to the presence of another phase (impurities) in our sample, i.e., 2Θ = 21.2° and 23.4°. The diffraction peak at 2Θ = 21.2° might be impurities of Cd-oleic due to the sample contain unreacted Cd-oleic precursor, which used in excess and is challenging to withdraw from the system. The diffraction peak at 2Θ = 23.4° might be due to the impurities of Se. Replacing (TOPO, HDA, OA) with (TBAI) ligand should not make any detectable changes in the position of the reflection peaks [62].

We concluded that, for our final goal of integrating these quantum dots in the photovoltaic device, the ligand exchange strategy is effective in preserving the quantum confinement and rendered the intact between the dots. We then employed the iodide treated CdSe nanoparticles in the fabrication of the bulk heterojunction solar cell by preparing a mixture blend of P3HT: PCBM: CdSe QDs. Our concept is to fabricate an inverted junction solar cell, and we applied the etched ITO electrode (work function 4.7) as a substrate for our device. We have then employed titanium dioxide layer as an electron blocking layer followed by the deposition of the active layer blend P3HT:CdSe:PCBM. To fully assemble the device structure, we evaporated a layer of molybdenum (IV) oxide MoO_3 thermally to serve as a hole-selective layer and finally Ag as top metal contact. Fig. 4 (a, b) present the characteristics J–V and EQE plots for the fabricated solar cell device. We compared the photovoltaic performance for a set of ITO/TiOx/P3HT: CdSe: PC60BM/MoO_3/Ag devices (red color) with another set of a control devices ITO/TiOx/P3HT: PC60BM/MoO_3/Ag (Black color) respectively. We finally summarized the extracted parameters from the J–V data in Table 2. The values of the J_{sc} are corrected based on the EQE measurements. Device with iodide capped QDs as an additive (ITO/TiOx/P3HT: CdSe: PC60BM/MoO_3/Ag) indicates a value of 7 .53 $mAcm^{-2}$ for the short circuit current(J_{sc}), 580 mV for the open-circuit voltage (V_{oc}) and 47% fill factor (*FF*) leading to a final Power conversion efficiency (*PCE*) of 2.5%. These values are compared with 6.48 $mAcm^{-2}$ for J_{sc}, 600 mV for $V_{oc}$and 42% FF with a PCE of 1.9% in the case of the controlled device (of ITO/TiOx/P3HT: PC60BM/MoO_3/Ag). The 31% increment in the power conversion efficiency is mainly corresponding to the increase in the values of the J_{sc} and FF upon using CdSe QDs as an additive in the device. Here, CdSe nanocrystal could facilitate the charge carrier's transport by bridging the separated island within the active layer blend, which accordingly results in more charge carrier's generation. The device structure, including a TEM image for the active layer blend and corresponding band diagram calculated according to Refs. [63,64] is shown in Fig. 4c.

4. Conclusion

We synthesized a colloidal CdSe quantum dots (QDs) using the organometallic method and employed it in the fabrication of inverted structure solar cells. We applied using poly (3-hexylthiophene) (P3HT) [6,6],-phenyl C61 butyric acid methyl ester (PC60BM) and TBAI capped CdSe QDs (P3HT:PC60BM: TBAI capped CdSe QDs) bulk heterojunction as an active layer for OSCs were successfully prepared. The photovoltaic performances of the cells with the (P3HT:PC60BM: TBAI capped CdSeQDs) are improved compared with the reference cells (P3HT: PC60BM). It has been revealed that the inserted of TBAI capped CdSe

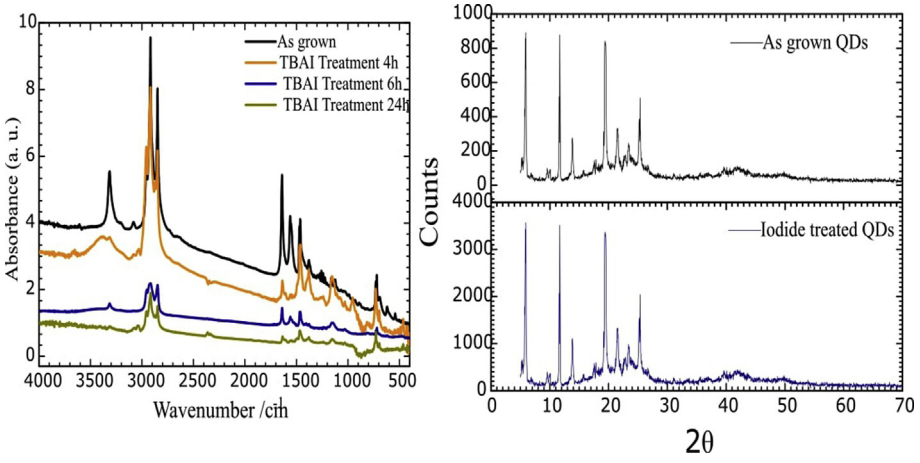

Fig. 3. (a) The Fourier transform infrared spectroscopy (FTIR) shows the changes in the vibronic modes upon treatment of the CdSe nanocrystal with the iodide ligand at a different time interval of 4 h, 6 h, and 24 h indicate the depletion of the TOPO/HDA/OA and the successive substitution by iodide ligand. (b) The X-ray diffraction pattern of the as-grownCdSe quantum dots and iodide treated dots.

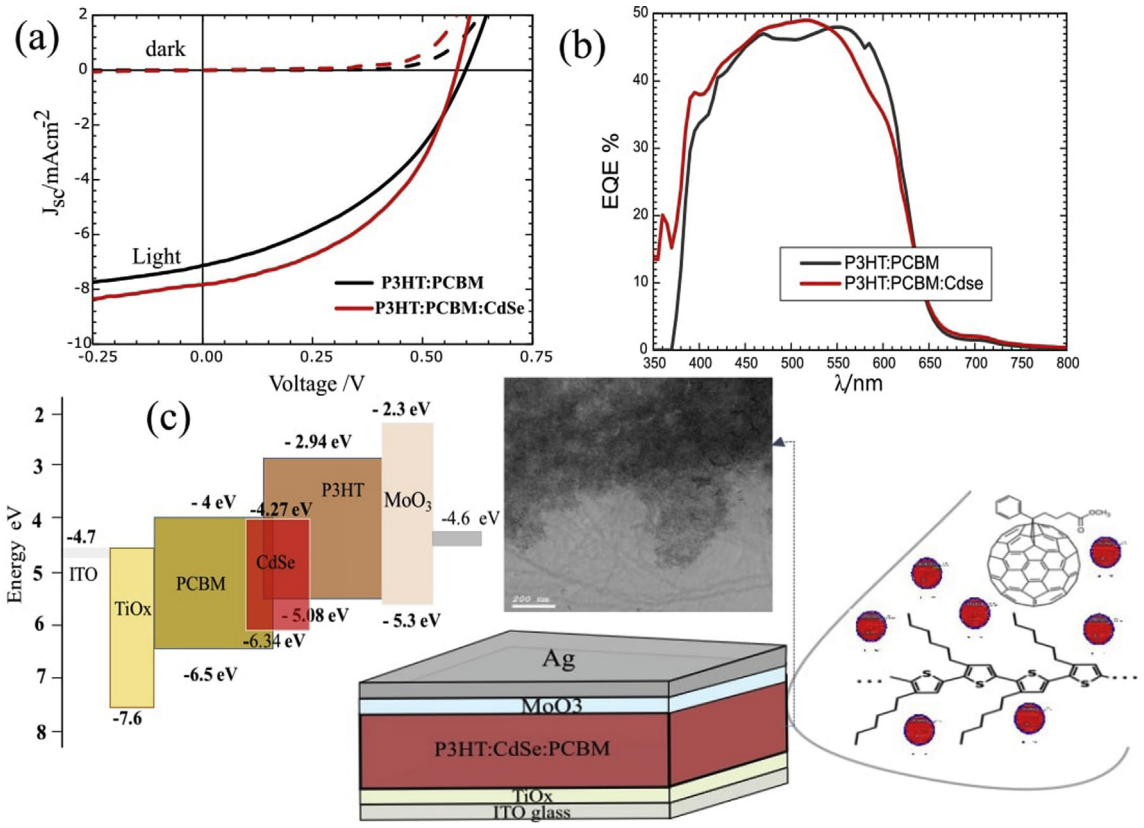

Fig. 4. (a) The J-V characteristics of ITO/TiOx/P3HT:PC60BM:CdSe/MoO_3/Ag (red) and ITO/TiOx/P3HT:PC60BM/MoO3/Ag (Black) Low temperature studies of the photoluminescence from colloidal CdSe nanocrystals prepared by the hot injection method in liquid paraffin shown in dark and under AM1.5 illuminations. (b) Spectral EQE characteristics of both devices. (C) Representation of the cell structure and the corresponding band diagram. It also shows a cartoon drawing for the active layer with CdSe QDs. (d) TEM image for P3HT: PCBM:CdSe QDs. (For interpretation of the references to color in this figure legend, the reader is referred to the Web version of this article.)

Table 2
Device parameters measured under illumination.

	Jsc [mA/cm²]	*Voc [V]*	*FF*	*Rs (Ω)*	*Rsh(Ω)*	*PCE (%)*
P3HT:PCBM	6.48 ± 0.01	0.6 ± 0.01	0.42 ± 0.02	300 ± 10	1250 ± 25	1.99 ± 0.2
P3HT:PCBM:CdSe	7.53 ± 0.03	0.58 ± 0.01	0.47 ± 0.01	200 ± 10	1890 ± 27	2.5 ± 0.15

QDs(size) on (P3HT: PC60BM) can improve the performance of the as-prepared OSCs. The measured PCE value of the (P3HT:PC60BM: TBAI capped CdSe QDs) device reaches up to 2.5%, while it is only 1.9% for the reference cell. We owe the performance improvement of the (P3HT:PC60BM: TBAI capped CdSe QDs(size) device to the band matching between the QDs and organic materials of the active layer and increased sunlight absorption in the visible range.

Declaration of competing interest

The authors declare that they have no known competing financial interests or personal relationships that could have appeared to influence the work reported in this paper.

Acknowledgment

Shaimaa A. Mohamed is grateful to Prof. Serdar Sariciftci and his research group for the continuous support providing the research facilities during her visit to Linz Institute of Organic Solar Cell (LIOS), Linz, Austria. Shaimaa. A. Mohamed and Salah. S. A. Obayya are acknowledging the financial support from the Academy of Scientific Research & Technology, Egypt in the framework of the Solar Energy Alliance project (ASRT-KTA).

Appendix A. Supplementary data

Supplementary data to this article can be found online at https://doi.org/10.1016/j.cap.2020.01.001.

References

[1] S. Das, J.-Y. Choi, T.L. Alford, P3HT:PC61BM based solar cells employing solution processed copper iodide as the hole transport layer, Sol. Energy Mater. Sol. Cells 133 (2015) 255–259, https://doi.org/10.1016/j.solmat.2014.11.004.
[2] W. Geens, T. Aernouts, J. Poortmans, G. Hadziioannou, Organic Co-evaporated Films of a PPV-Pentamer and C 60 : Model Systems for Donor Y Acceptor Polymer Blends vol 404, (2002), pp. 438–443.
[3] A. Fischer, L. Rollny, J. Pan, G.H. Carey, S.M. Thon, S. Hoogland, O. Voznyy, D. Zhitomirsky, J.Y. Kim, O.M. Bakr, E.H. Sargent, Directly deposited quantum dot solids using a colloidally stable nanoparticle ink, Adv. Mater. 25 (2013) 5742–5749, https://doi.org/10.1002/adma.201302147.
[4] M.N. Amalina, N.A. Rasheid, M. Rusop, The properties of sprayed nanostructured P-Type CuI films for dye-sensitized solar cells application, J. Nanomater. 2012 (2012), https://doi.org/10.1155/2012/637637.
[5] L. Qiu, J. Deng, X. Lu, Z. Yang, H. Peng, Integrating perovskite solar cells into a flexible fiber, Angew. Chem. Int. Ed. 53 (2014) 10425–10428, https://doi.org/10.1002/anie.201404973.
[6] A.R.B.M. Yusoff, M.K. Nazeeruddin, Organohalide lead perovskites for photovoltaic

applications, J. Phys. Chem. Lett. (2016), https://doi.org/10.1021/acs.jpclett.5b02893.
[7] J. Weickert, H. Sun, C. Palumbiny, H.C. Hesse, L. Schmidt-Mende, Spray-deposited PEDOT:PSS for inverted organic solar cells, Sol. Energy Mater. Sol. Cells (2010), https://doi.org/10.1016/j.solmat.2010.08.018.
[8] A. Stapleton, B. Vaughan, B. Xue, E. Sesa, K. Burke, X. Zhou, G. Bryant, O. Werzer, A. Nelson, A.L. David Kilcoyne, L. Thomsen, E. Wanless, W. Belcher, P. Dastoor, A multilayered approach to polyfluorene water-based organic photovoltaics, Sol. Energy Mater. Sol. Cells 102 (2012) 114–124, https://doi.org/10.1016/j.solmat.2012.03.016.
[9] N.C. Giebink, G.P. Wiederrecht, M.R. Wasielewski, S.R. Forrest, Thermodynamic efficiency limit of excitonic solar cells, Phys. Rev. B Condens. Matter Mater. Phys. 83 (2011) 1–6, https://doi.org/10.1103/PhysRevB.83.195326.
[10] G. Li, V. Shrotriya, J. Huang, Y. Yao, T. Moriarty, K. Emery, Y. Yang, High-efficiency solution processable polymer photovoltaic cells by self-organization of polymer blends, Nat. Mater. (2005), https://doi.org/10.1038/nmat1500.
[11] W. Yue, X. Huang, J. Yuan, W. Ma, F.C. Krebs, D. Yu, A novel benzodipyrrolidone-based low band gap polymer for organic solar cells, J. Mater. Chem. A. 1 (2013) 10116–10119, https://doi.org/10.1039/c3ta12701j.
[12] D. Yu, K. Park, M. Durstock, L. Dai, Fullerene-grafted graphene for efficient bulk heterojunction, Polymer Photovoltaic Devices 26 (2011) 1113–1118.
[13] T. Chu, J. Lu, S. Beaupr, Y. Zhang, Bulk heterojunction solar cells using thieno[3,4-c]pyrrole-4,6-dione and dithieno[3,2-b:20,30-d]silole copolymer with a power conversion efficiency of 7.3%, J. Am. Chem. Soc. 133 (2011) 4250–4253.
[14] S. Fabiano, Z. Chen, S. Vahedi, a. Facchetti, B. Pignataro, M.a. Loi, Role of photoactive layer morphology in high fill factor all-polymer bulk heterojunction solar cells, J. Mater. Chem. 21 (2011) 5891, https://doi.org/10.1039/c0jm03405c.
[15] L. Ma, Y. Xu, Y. Zu, Q. Liao, B. Xu, C. An, S. Zhang, J. Hou, A ternary organic solar cell with 300 nm thick active layer shows over 14% efficiency, Sci. China Chem. (2019) 1–7, https://doi.org/10.1007/s11426-019-9556-7.
[16] C. Winder, Sensitization of Low Bandgap Polymer Bulk Heterojunction Solar Cells, (2001).
[17] T. Rousseau, A. Cravino, T. Bura, G. Ulrich, R. Ziessel, J. Roncali, BODIPY derivatives as donor materials for bulk heterojunction solar cells, Chem. Commun. (2009) 1673–1675, https://doi.org/10.1039/b822770e.
[18] O.S. Cells, A.W. Hassel, Doping Induced Effects in Organic Semiconductors and Bulk Heterojunctions, (2013).
[19] R. Des, R. Eines, R. Im, Bulk-heterojunction Hybrid Solar Cells Based on Colloidal CdSe Quantum Dots and Conjugated Polymers, (2011).
[20] F. Yang, M. Shtein, S.R. Forrest, Controlled growth of a molecular bulk heterojunction photovoltaic cell, Nat. Mater. (2005), https://doi.org/10.1038/nmat1285.
[21] Nanoscale morphology of conjugated polymer/fullerene-based bulk- heterojunction solar cells, Adv. Funct. Mater. 14 (2004) 1005–1011, https://doi.org/10.1002/adfm.200305026 , Accessed date: 30 January 2013https://search.crossref.org/?q=Nanoscale+morphology+of+conjugated+polymer%2Ffullerene-based+bulk-+heterojunction+solar+cells.
[22] M. He, W. Han, J. Ge, W. Yu, Y. Yang, F. Qiu, Z. Lin, Annealing effects on the photovoltaic performance of all-conjugated poly(3-alkylthiophene) diblock copolymer-based bulk heterojunction solar cells, Nanoscale 3 (2011) 3159–3163, https://doi.org/10.1039/c1nr10293a.
[23] N. Shintaku, M. Hiramoto, S. Izawa, Doping for controlling open-circuit voltage in organic solar cells, J. Phys. Chem. C 122 (2018) 5248–5253, https://doi.org/10.1021/acs.jpcc.7b12203.
[24] J. Li, Z. Liang, Y. Peng, J. Lv, X. Ma, Y. Wang, Y. Xia, 36% enhanced efficiency of Ternary Organic Solar Cells by Doping a NT-based polymer as an electron-cascade donor, Polymers 10 (2018) 1–11, https://doi.org/10.3390/polym10070703.
[25] I. Salzmann, G. Heimel, M. Oehzelt, S. Winkler, N. Koch, Molecular electrical doping of organic semiconductors: fundamental mechanisms and emerging dopant design rules, Acc. Chem. Res. 49 (2016) 370–378, https://doi.org/10.1021/acs.accounts.5b00438.
[26] M.L. Tietze, J. Benduhn, P. Pahner, B. Nell, M. Schwarze, H. Kleemann, M. Krammer, K. Zojer, K. Vandewal, K. Leo, Elementary steps in electrical doping of organic semiconductors, Nat. Commun. 9 (2018) 1–8, https://doi.org/10.1038/s41467-018-03302-z.
[27] Z. Ahmad, M.A. Najeeb, R.A. Shakoor, S.A. Al-Muhtaseb, F. Touati, Limits and possible solutions in quantum dot organic solar cells, Renew. Sustain. Energy Rev. 82 (2018) 1551–1564, https://doi.org/10.1016/j.rser.2017.07.001.
[28] H. Lim, K.S. Lee, Y. Liu, H.Y. Kim, D.I. Son, Photovoltaic performance of inverted polymer solar cells using hybrid carbon quantum dots and absorption polymer materials, Electron. Mater. Lett. 14 (2018) 581–586, https://doi.org/10.1007/s13391-018-0064-8.
[29] J.M. Lee, B.-H. Kwon, H. Il Park, H. Kim, M.G. Kim, J.S. Park, E.S. Kim, S. Yoo, D.Y. Jeon, S.O. Kim, Exciton dissociation and charge-transport enhancement in organic solar cells with quantum-dot/N-doped CNT hybrid nanomaterials, Adv. Mater. 25 (2013) 2011, https://doi.org/10.1002/adma.201204454 –7.
[30] M. Mehrabian, R.M. Jahandizi, Improvement of energy harvesting with PbS quantum dots in novel structure of organic solar cells, J. Nanoelectron. Optoelectron. 10 (2015) 633–637, https://doi.org/10.1166/jno.2015.1821.
[31] R. Mastria, A. Rizzo, C. Giansante, D. Ballarini, L. Dominici, O. Inganäs, G. Gigli, Role of polymer in hybrid polymer/PbS quantum dot solar cells, J. Phys. Chem. C 119 (2015) 14972–14979, https://doi.org/10.1021/acs.jpcc.5b03761.
[32] Y. Wang, L. Yan, G. Ji, C. Wang, H. Gu, Q. Luo, Q. Chen, L. Chen, Y. Yang, C.Q. Ma, X. Liu, Synthesis of N,S-doped carbon quantum dots for use in organic solar cells as the ZnO modifier to eliminate the light-soaking effect, ACS Appl. Mater. Interfaces 11 (2019) 2243–2253, https://doi.org/10.1021/acsami.8b17128.
[33] R. Kang, S. Park, Y.K. Jung, D.C. Lim, M.J. Cha, J.H. Seo, S. Cho, High-efficiency polymer homo-tandem solar cells with carbon quantum-dot-doped tunnel junction intermediate layer, Adv. Energy Mater. 8 (2018) 1–8, https://doi.org/10.1002/aenm.201702165.
[34] J. Park, S. Hwang, S. Jeong, S. Kim, J. Bang, S. Cho, Heterojunction area-controlled inorganic nanocrystal solar cells fabricated using supra-quantum dots, ACS Appl. Mater. Interfaces 10 (2018) 43768–43773, https://doi.org/10.1021/acsami.8b14752.
[35] S.J. Oh, N.E. Berry, J.H. Choi, E.A. Gaulding, T. Paik, S.H. Hong, C.B. Murray, C.R. Kagan, Stoichiometric control of lead chalcogenide nanocrystal solids to enhance their electronic and optoelectronic device performance, ACS Nano 7 (2013) 2413–2421, https://doi.org/10.1021/nn3057356.
[36] I. Lokteva, N. Radychev, F. Witt, H. Borchert, J. Parisi, J. Kolny-Olesiak, Surface treatment of cdse nanoparticles for application in hybrid solar cells: the effect of multiple ligand exchange with pyridine, J. Phys. Chem. C 114 (2010) 12784–12791, https://doi.org/10.1021/jp103300v.
[37] S.W. Baek, S. Jun, B. Kim, A.H. Proppe, O. Ouellette, O. Voznyy, C. Kim, J. Kim, G. Walters, J.H. Song, S. Jeong, H.R. Byun, M.S. Jeong, S. Hoogland, F.P. García de Arquer, S.O. Kelley, J.Y. Lee, E.H. Sargent, Efficient hybrid colloidal quantum dot/organic solar cells mediated by near-infrared sensitizing small molecules, Nat. Energy. 4 (2019) 969–976, https://doi.org/10.1038/s41560-019-0492-1.
[38] J. Albero, P. Riente, J.N. Clifford, M.A. Pericàs, E. Palomares, Improving CdSe quantum dot/polymer solar cell efficiency through the covalent functionalization of quantum dots: implications in the device recombination kinetics, J. Phys. Chem. C 117 (2013) 13374–13381, https://doi.org/10.1021/jp403523j.
[39] E.K. Park, J.H. Kim, I.A. Ji, H.M. Choi, J.H. Kim, K.T. Lim, J.H. Bang, Y.S. Kim, Optimization of CdSe quantum dot concentration in P3HT:PCBM layer for the improved performance of hybrid solar cells, Microelectron. Eng. 119 (2014) 169–173, https://doi.org/10.1016/j.mee.2014.05.003.
[40] S.A. Jotterand, M. Jobin, Characterization of P3HT:PCBM:CdSe hybrid solar cells, Energy Procedia 31 (2011) 117–123, https://doi.org/10.1016/j.egypro.2012.11.173.
[41] F. Ongul, S.A. Yuksel, C. Allahverdi, S. Bozar, M. Kazici, S. Gunes, Influences of CdSe NCs on the photovoltaic parameters of BHJ organic solar cells, Spectrochim. Acta Part A Mol. Biomol. Spectrosc. 194 (2018) 50–56, https://doi.org/10.1016/j.saa.2018.01.012.
[42] N.T.N. Truong, W.K. Kim, C. Park, Effect of CdSe/P3HT composition on electrical and structural properties of bulk hetero-junction solar cell active layer, Sol. Energy Mater. Sol. Cells (2011), https://doi.org/10.1016/j.solmat.2010.05.017.
[43] S. Ren, L.-Y. Chang, S.-K. Lim, J. Zhao, M. Smith, N. Zhao, V. Bulović, M. Bawendi, S. Gradecak, Inorganic-organic hybrid solar cell: bridging quantum dots to conjugated polymer nanowires, Nano Lett. 11 (2011) 3998–4002, https://doi.org/10.1021/nl202435t.
[44] M.J. Greaney, S. Das, D.H. Webber, S.E. Bradforth, R.L. Brutchey, Improving open circuit potential in hybrid P3HT: CdSe bulk heterojunction solar cells via colloidal tert-butylthiol ligand exchange, ACS Nano 6 (2012) 4222–4230, https://doi.org/10.1021/nn3007509.
[45] J. Tang, K.W. Kemp, S. Hoogland, K.S. Jeong, H. Liu, L. Levina, M. Furukawa, X. Wang, R. Debnath, D. Cha, K.W. Chou, A. Fischer, A. Amassian, J.B. Asbury, E.H. Sargent, Colloidal-quantum-dot photovoltaics using atomic-ligand passivation, Nat. Mater. 10 (2011) 765–771, https://doi.org/10.1038/nmat3118.
[46] M. Zanella, L. Maserati, M. Pernia Leal, M. Prato, R. Lavieville, M. Povia, R. Krahne, L. Manna, Atomic ligand passivation of colloidal nanocrystal films via their reaction with propyltrichlorosilane, Chem. Mater. 25 (2013) 1423–1429, https://doi.org/10.1021/cm303022w.
[47] W.K. Bae, J. Joo, L.A. Padilha, J. Won, D.C. Lee, Q. Lin, W.K. Koh, H. Luo, V.I. Klimov, J.M. Pietryga, Highly effective surface passivation of pbse quantum dots through reaction with molecular chlorine, J. Am. Chem. Soc. 134 (2012) 20160–20168, https://doi.org/10.1021/ja309783v.
[48] J.H. Ko, D. Yoo, Y.H. Kim, Atomic models for anionic ligand passivation of cation-rich surfaces of IV-VI, II-VI, and III-V colloidal quantum dots, Chem. Commun. 53 (2017) 388–391, https://doi.org/10.1039/c6cc07933d.
[49] M.M. Tavakoli, Surface engineering of pbs colloidal quantum dots using atomic passivation for photovoltaic applications, Procedia Eng 139 (2016) 117–122, https://doi.org/10.1016/j.proeng.2015.08.1122.
[50] D. Bederak, D.M. Balazs, N.V. Sukharevska, A.G. Shulga, M. Abdu-Aguye, D.N. Dirin, M.V. Kovalenko, M.A. Loi, Comparing halide ligands in PbS colloidal quantum dots for field-effect transistors and solar cells, ACS Appl. Nano Mater. 1 (2018) 6882–6889, https://doi.org/10.1021/acsanm.8b01696.
[51] H. Lu, J. Joy, R.L. Gaspar, S.E. Bradforth, R.L. Brutchey, Iodide-passivated colloidal PbS nanocrystals leading to highly efficient polymer:nanocrystal hybrid solar cells, Chem. Mater. 28 (2016) 1897–1906, https://doi.org/10.1021/acs.chemmater.6b00185.
[52] Y. Cao, A. Stavrinadis, T. Lasanta, D. So, G. Konstantatos, The role of surface passivation for efficient and photostable PbS quantum dot solar cells, Nat. Energy. 1 (2016) 1–6, https://doi.org/10.1038/NENERGY.2016.35.
[53] W.W. Yu, L. Qu, W. Guo, X. Peng, Experimental determination of the extinction coefficient of CdTe, CdSe, and CdS nanocrystals, Chem. Mater. 15 (2003) 2854–2860, https://doi.org/10.1021/cm034081k.
[54] J.Y. Kim, S.H. Kim, H.H. Lee, K. Lee, W. Ma, X. Gong, A.J. Heeger, New architecture for high-efficiency polymer photovoltaic cells using solution-based titanium oxide as an optical spacer, Adv. Mater. 18 (2006) 572–576, https://doi.org/10.1002/adma.200501825.
[55] H. Hassan, T. Abdallah, S. Negm, H. Talaat, Rabi like angular splitting in surface plasmon polariton – exciton interaction in ATR configuration, Appl. Surf. Sci. 441 (2018) 341–346, https://doi.org/10.1016/j.apsusc.2018.02.020.
[56] E.J.D. Klem, H. Shukla, S. Hinds, D.D. Macneil, L. Levina, E.H. Sargent, Impact of

Dithiol Treatment and Air Annealing on the Conductivity , Mobility , and Hole Density in PbS Colloidal Quantum Dot Solids, (2008), pp. 100–102, https://doi.org/10.1063/1.2917800.
[57] D.V. Talapin, S. Haubold, A.L. Rogach, A. Kornowski, M. Haase, H. Weller, A novel organometallic synthesis of highly luminescent CdTe nanocrystals, J. Phys. Chem. B 105 (2001) 2260–2263, https://doi.org/10.1021/jp003177o.
[58] M. Thambidurai, N. Murugan, Preparation and characterization of nanocrystalline CdS Thin films, Chalcogenide Lett. 6 (2009) 171–179 http://chalcogen.ro/171_Thambidurai.pdf , Accessed date: 2 September 2014.
[59] O. (Otfried) Madelung, Semiconductors : Data Handbook, Springer, 2004.
[60] V.A. Online, G. Niu, L. Wang, R. Gao, W. Li, X. Guo, H. Dong, Y. Qiu, Inorganic halogen ligands in quantum dots : I À, Br À (2013) 19595–19600, https://doi.org/10.1039/c3cp52678j.
[61] G. Niu, L. Wang, R. Gao, W. Li, X. Guo, H. Dong, Y. Qiu, Inorganic halogen ligands in quantum dots: I-, Br-, Cl- and film fabrication through electrophoretic deposition, Phys. Chem. Chem. Phys. 15 (2013) 19595–19600, https://doi.org/10.1039/c3cp52678j.
[62] N.T.N. Truong, W.K. Kim, U. Farva, X.D. Luo, C. Park, Improvement of CdSe/P3HT bulk hetero-junction solar cell performance due to ligand exchange from TOPO to pyridine, Sol. Energy Mater. Sol. Cells 95 (2011) 3009–3014, https://doi.org/10.1016/j.solmat.2011.06.015.
[63] J. Jasieniak, J. Pacifico, R. Signorini, A. Chiasera, M. Ferrari, A. Martucci, P. Mulvaney, Luminescence and amplified stimulated emission in CdSe-ZnS-nanocrystal- doped TiO2 and ZrO2 waveguides, Adv. Funct. Mater. 17 (2007) 1654–1662, https://doi.org/10.1002/adfm.200600955.
[64] M. Mall, P. Kumar, S. Chand, L. Kumar, Influence of ZnS quantum dots on optical and photovoltaic properties of poly(3-hexylthiophene), Chem. Phys. Lett. 495 (2010) 236–240, https://doi.org/10.1016/j.cplett.2010.06.067.